

# Measurement of particle motion in optical tweezers embedded in a Sagnac interferometer

Ivan Galinskiy <sup>\*1,2</sup>, Oscar Isaksson<sup>1,3</sup>, Israel Rebolledo Salgado<sup>1,4</sup>, Mathieu Hautefeuille<sup>2</sup>, Bernhard Mehlig<sup>1</sup>, and Dag Hanstorp<sup>1</sup>

<sup>1</sup>Department of Physics, University of Gothenburg, SE-412 96 Gothenburg, Sweden

<sup>2</sup>Faculty of Sciences, National Autonomous University of Mexico, 04510, Mexico City, Mexico

<sup>3</sup>Department of Applied physics, Chalmers University of Technology, SE-412 96 Gothenburg, Sweden

<sup>4</sup>Instituto de Ciencias Físicas, National Autonomous University of Mexico, 62210, Cuernavaca, Mexico

## Abstract

We have constructed a counterpropagating optical tweezers setup embedded in a Sagnac interferometer in order to increase the sensitivity of position tracking for particles in the geometrical optics regime. The enhancement of the position determination using a Sagnac interferometer has previously been described theoretically by Taylor *et al.* [Journal of Optics 13, 044014 (2011)] for Rayleigh-regime particles trapped in an antinode of a standing wave. We have extended their theory to a case of arbitrarily-sized particles trapped with orthogonally-polarized counterpropagating beams. The working distance of the setup was sufficiently long to optically induce particle oscillations orthogonally to the axis of the tweezers with an auxiliary laser beam. Using these oscillations as a reference, we have experimentally shown that Sagnac-enhanced back focal plane interferometry is capable of providing an improvement of more than 5 times in the signal-to-background ratio, corresponding to a more than 30-fold improvement of the signal-to-noise ratio. The obtained results are consistent with our theoretical predictions. In the experimental setup, we used a method of optical levitator-assisted liquid droplet delivery in air based on commercial inkjet technology, with a novel method to precisely control the size of droplets.

## 1 Introduction

The techniques of optical levitation and optical tweezers were introduced by A. Ashkin *et al.* in 1971 and 1986, respectively [1, 2]. In optical levitation, a weakly focused vertically aligned laser beam creates an optical pressure force on a dielectric particle which can become sufficiently strong to compensate gravity. A weak gradient force provides stability in the horizontal plane, creating a stable trap. In optical tweezers, on the other hand, a tightly focused beam is used to provide stable trapping even in the absence of external forces, giving a trapping position that is independent of the laser power.

One of the most important properties of optical tweezers is that they offer the possibility to precisely measure the position of a trapped particle. This is useful, for example, in single-molecule tracking in microbiology [10] or in cooling of vibrational degrees of freedom in statistical physics experiments [6]. The standard method for tracking the position of a particle in optical tweezers is back focal plane (BFP) interferometry in which the back focal plane of the condenser lens is imaged onto a quadrant photodiode detector (QPD) [4]. While back focal plane interferometry allows for very high resolution in the tracking of micron-scale particles [10], it is subject to shot noise as any other optical method of measurement. This ultimately limits the resolution of position measurements for particles of any size. The limiting effects of shot noise on position measurement of Rayleigh-regime particles ( $d \ll \lambda$ ) were shown by Taylor *et al.* [11], where the

---

\*Corresponding author. Email address: [iv.galinskiy@ciencias.unam.mx](mailto:iv.galinskiy@ciencias.unam.mx)

particle was assumed to be trapped in an antinode of the beating pattern produced by same-polarization counterpropagating beams.

The general problem of enhancing the signal-to-noise ratio for position measurements of the trapped particle can be mitigated by using a counterpropagating optical tweezers setup embedded in a Sagnac interferometer. In counterpropagating optical tweezers, two opposite-travelling trapping beams are focused into the same focal point [8] by a pair of lenses. By embedding such a setup into a Sagnac interferometer, it is possible to selectively attenuate the trapping field, while preserving the asymmetrical field components that carry information about the position of the particle, thus increasing the signal-to-background ratio and consequently, the signal-to-noise ratio. This was shown theoretically by Taylor *et al.* [11], with results applicable to Rayleigh scatterers, i.e. dielectric particles much smaller than the wavelength of light, trapped at an antinode.

There are many applications that use particles that are comparable to or larger than the wavelength of trapping light, being in the Mie or the geometrical optics regime [6, 10], where the trapping is achieved with orthogonally polarized counterpropagating beams to minimize beating effects. These applications could benefit from the Sagnac-enhanced position measuring sensitivity, for which we generalize the theory by Taylor *et al.* [11] to arbitrary-size spherical particles in a setup where the counterpropagating beams are *orthogonally* polarized, after which we confirm the enhanced signal-to-noise ratio experimentally. The reflections from the particle itself and other optical surfaces in the system are detrimental to the signal-to-noise ratio. In our setup they are successfully eliminated by polarization filtering in the interferometer. The same technique also allows to compensate for splitting inequalities in the beamsplitter.

We implemented a technique for high-efficiency single-droplet generation in air based on a commercial inkjet cartridge [9] and evaporation-based diameter adjustment that allowed us to create droplets with precise control over their size. The trapping was greatly simplified by using levitator-assisted particle delivery into the optical tweezers [3, 5]. The long working distance (WD) of the aspherical lenses used for the optical tweezers simplified the optical access to the trapped particle from a direction perpendicular to the optical axis of the tweezers. This allowed us to optically induce oscillations of the trapped particle orthogonally to the trapping beam using a modulated “side-pressure” laser beam, which served as a reference for signal-to-background measurements. The obtained results closely matched our theoretical predictions.

## 2 Experimental setup

Figure 1 shows the main part of the optical system, and figure 2 shows the details of the interaction region located between the mirrors M2 and M3 in figure 1. First in this section a short description of the experimental procedure will be presented, after which the different parts will be described in detail. An experiment is initiated by emitting droplets from a commercial inkjet cartridge (HP C6614), shown as the gray box in figure 2. The droplet descends towards a vertically oriented levitator beam (figure 3) where it is trapped above the level of the horizontal laser beams of the optical tweezers, as shown on figure 4a. The power in the levitator is then reduced to lower the particle, while the power in the horizontal lasers beams is increased. This effectively lowers the droplet until it descends into the counterpropagating optical tweezers (figure 4b), where it is stably trapped. After that, all the light is coupled into the optical tweezers (figure 4c). Finally, the side-pressure laser (shown as the blue beam in figure 2) is enabled and pulsed at a chosen frequency. This pushes the particle out of its equilibrium position, and its subsequent motion is monitored using a Quadrant Photodiode Detector (QPD).

### 2.1 Droplet generation using an inkjet cartridge

We have constructed a system for generating droplets of controllable size using an inkjet cartridge. The system is based on some of the methods demonstrated in [5, 9]. A commercial black inkjet cartridge was emptied and washed several times with distilled water. Our technique of droplet size control consists in filling the cartridge with a 5% solution of glycerol in water. While the diameter of the particles emitted by the cartridge was measured to be a nearly constant  $34 \mu\text{m}$ , the quick evaporation of water from the falling

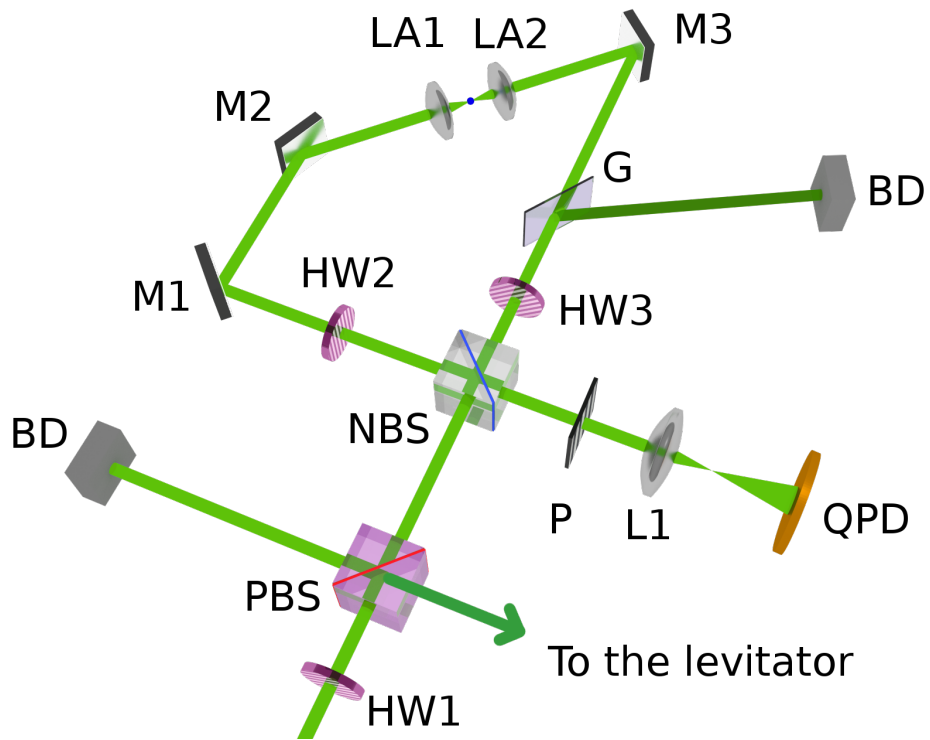


Figure 1: The optical setup of the optical tweezers subsystem. HW - half-wave plate, PBS - polarizing beamsplitter, NBS - non-polarizing beamsplitter, BD - beam dump, L - lens, P - polarizer, G - glass plate, LA - aspherical lens, M - mirror

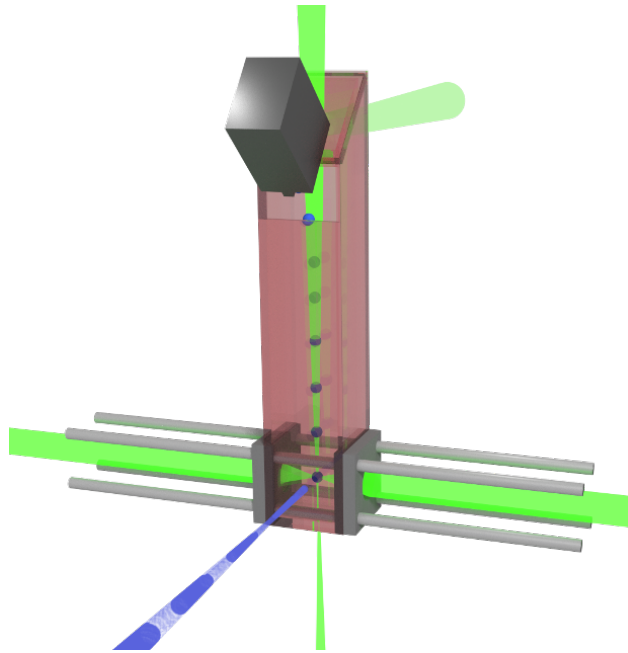


Figure 2: A schematic close-up of the trapping point together with the glass cell. The cartridge (gray box) generates droplets that descend vertically through the levitation beam (vertical green beam) until they are trapped in the counterpropagating optical tweezers (horizontal green beams), where they are perturbed horizontally by a TTL-modulated laser (blue horizontal beam). The top glass plate is tilted to direct the Fresnel reflections out of the cell.

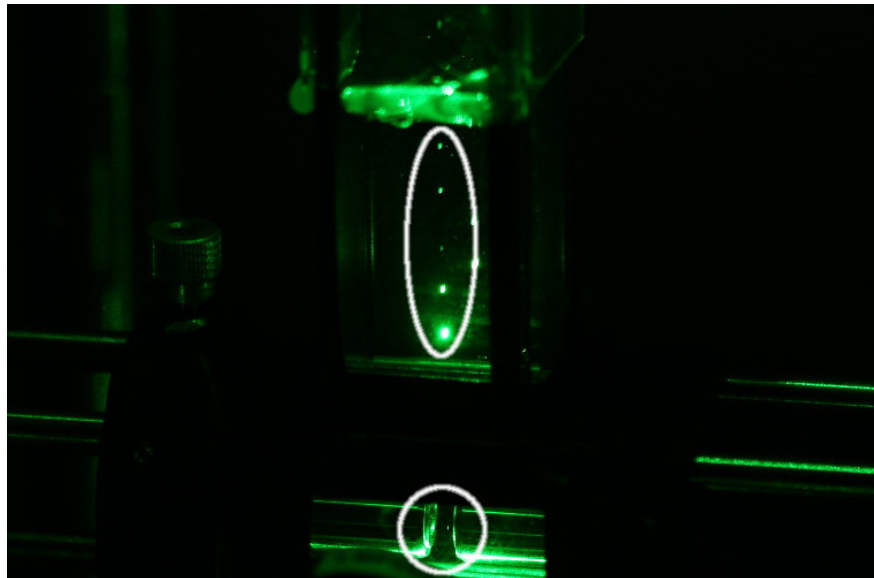


Figure 3: Several droplets (in the upper ellipse) descending through the levitator beam towards the trapping point of the optical tweezers (in the lower circle)

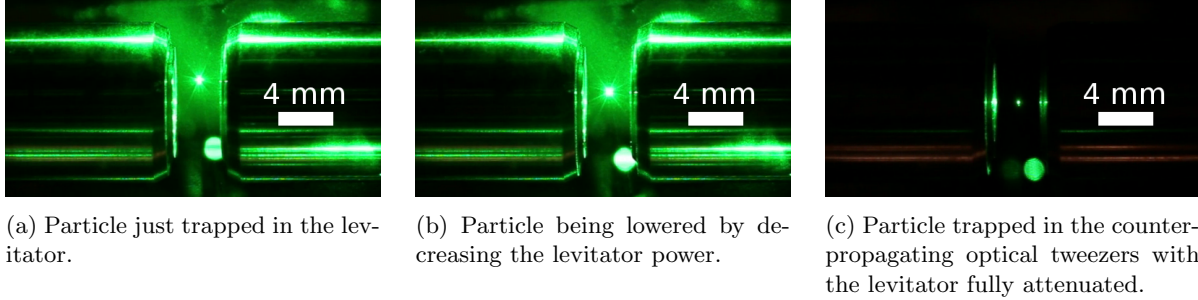


Figure 4: Successive steps in trapping

droplets reduces the diameter to  $11 \pm 1 \mu\text{m}$ . This size is more suitable for trapping due to a lower mass, while still being larger than the wavelength of trapping light.

The cartridge had to be positioned out of line of the vertical levitation laser beam to avoid high-intensity light from reaching the cartridge surface and creating serious convection flows in the cell and damage in the cartridge itself. In order for the droplets to reach the levitator beam, the cartridge was tilted at an angle of approximately  $45^\circ$  with respect to the horizontal plane (figure 2). Then, the ejected droplets fly 3-5 cm at an angle of  $45^\circ$  before reaching their terminal velocity, which allows them to reach the levitation beam and descend vertically afterwards (figure 3). With proper protection against air currents, the droplets fall predictably into the focal region of the levitation beam where the optical pressure is sufficient for stable levitation.

## 2.2 Trapping cell

The main purpose of the trapping cell is to shield the droplets from external air currents. Additionally it allows the levitation light beam to pass through the setup without reflecting it back into the cell and creating convection flows. This was achieved by tilting the upper glass plate  $45^\circ$  (figure 2) to allow the Fresnel reflections to be deflected, and placing a beam dump outside the cell. The cell is sufficiently tall to guarantee the full evaporation of the solvent (water) in the particles, allowing them to achieve the desired diameter prior to trapping. The trapping cell was constructed with microscope slides sustained by the optical cage system that is also holding the lens assembly, as shown in figures 2 and 3.

## 2.3 Optical levitator

The light in the optical setup is generated by a DPSS green laser module (Laser Quantum, 532 nm, 2 W maximum power). The output beam is split by a polarizing beamsplitter into two beams (PBS in figure 1), where the split ratio is controlled by rotating the half-wave plate HW1. The transmitted part is guided into the optical tweezers system shown in figure 1, and the other part is guided into the optical levitation system, entering from below in figure 2.

The optical levitator beam, directed vertically, was focused with a  $f=100$  mm lens to create a focal point slightly below the optical tweezers such that the focal point of the levitator beam was about 2 mm below the optical tweezers' trapping point (figure 2). The focal spot diameter of the Gaussian levitation beam was calculated to be  $17 \mu\text{m}$ . The stable trapping point of the levitator when using 1000 mW of laser power is located approximately 4 mm above the focal point of the levitator beam, and hence 2 mm above the focal point of the optical tweezers.

## 2.4 Optical tweezers

The p-polarized beam from the laser enters the non-polarizing beamsplitter NBS where it is split into one clockwise (CW) and one counterclockwise (CCW) beams. The CCW beam becomes s-polarized after passing

through the half-wave plate HW3, which is rotated at  $45^\circ$  from the horizontal plane. After that, the glass plate G tilted at approximately Brewster’s angle reflects a part of the CCW beam, thus compensating for a power disbalance between the CW and CCW beams caused by the NBS beamsplitter (Thorlabs BSW26). Then, after one reflection the beam passes through the aspherical lens LA2, where it is focused onto the particle. Both lenses are aligned to make the focal points coincide, which will be the trapping position for the particle. After the beam passes through the particle, it is collimated again by the lens LA1. The focused cone of light has a numerical aperture of 0.30.

The CW beam, on the other hand, first passes through the aspherical lenses and then through the glass plate G. However, since it is p-polarized, and the angle of G is close to Brewster’s angle, only a slight fraction of this beam is reflected. In this way both beams not only have the same power at the trapping point, but also when ”meeting” at NBS. Finally, the CW field passes through HW3 which converts it from p-polarized to s-polarized.

Therefore, both the CW and CCW beams are s-polarized when combined again at NBS. Note that the fast axis of the half-wave plate HW2 is horizontal and thus, simply compensates for the additional  $\pi$  phase shift between the different polarizations caused by the mirrors and the HW2 waveplate.

After recombining at NBS, the combined beams interfere destructively when travelling towards the quadrant photodiode (QPD), thus creating the so-called ”dark port” of the interferometer and interfere constructively when travelling back towards the laser. There, since all the reflected light returning to the beamsplitter is p-polarized, a polarizer (P) eliminates nearly all the light that was reflected either from the surface of the particle or from the optical components in the setup. Finally, a lens (L) images the back focal planes of both lenses onto the QPD.

Note that a Sagnac interferometer usually creates a severe backreflection problem because of the constructive interference in the beam returning to the laser. However, in this setup the backreflected beam is polarized orthogonally to the input beam, and it is possible to filter all the backreflected light in the PBS polarizing beamsplitter, directing it to the beam dump BD.

In order to compare the performance of the Sagnac-enhanced position sensing to the usual back focal plane interferometry method, we take advantage of a ghost reflection from the NBS beamsplitter. This ghost reflection has the property of being a highly attenuated sample of the CW-propagating beam only. By blocking the dark port field and opening the ghost reflection (or vice versa), it’s possible to conveniently ”switch“ between the two modes of operation while using the same imaging lens (L).

## 2.5 Horizontal pressure laser

The system to induce horizontal oscillations of the trapped particle is conceptually similar to the optical levitator described above. A separate DPSS laser (532 nm, 200 mW) is controlled by a Pulse Width Modulated (PWM) signal with a given frequency (0-10 kHz) and a controllable duty cycle. Its output is steered and focused horizontally onto the trapped particle (figure 2). The beam waist is deliberately located slightly behind the particle in order to reduce the total optical force produced by the side beam. The Airy-like diffraction pattern produced after passing through the trapping point with a trapped particle (figure 5) indicates that the beam is incident on the particle and thus confirms the correct alignment.

## 2.6 Particle size measurement

In order to measure the trapped particle size, we use the ”side-pressure“ beam at low power and record the resulting diffraction pattern (figure 5). The distance between the minima, then, gives a size estimate for the particle. The size was measured to be  $11 \pm 1 \mu\text{m}$ .

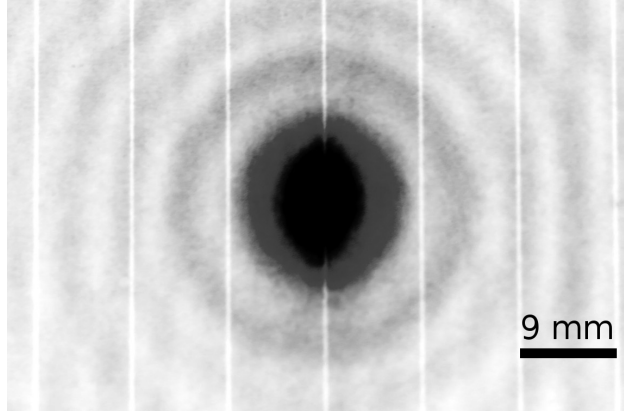


Figure 5: Airy pattern produced by the side-pressure laser passing through the trapped particle (inverted colors) and recorded at a distance of 10.5 cm from the trapping spot. The bright central spot is unscattered laser light and the thin vertical stripes are markings on the surface of the screen for scale calibration.

## 3 Theory

### 3.1 Assumptions and definitions

The experiment proposed by Taylor *et al.* [11] assumes the trapped particle to be a Rayleigh scatterer, i.e. a dielectric particle significantly smaller than the wavelength of the trapping light. We generalized their theory to a case of a homogeneous spherical particle of arbitrary size.

The time dependence of the fields is dropped. A coordinate system is defined for each beam to have  $\hat{z}$  along the beam propagation (with different signs for the CW and CCW beams),  $\hat{y}$  pointing out of the plane in which the interferometer is located (for example, a plane parallel to the optical table) and  $\hat{x} = \hat{y} \times \hat{z}$ . Additionally, we drop the  $y$ -component dependence of the fields, i.e.  $\phi(x, y) \equiv \phi(x)$  since we investigate only the signal improvement in the  $x$ -direction. For a compact and clear notation, we describe the propagation of the fields through the system with operators, following the method introduced in Ref. [7]. For example, to handle the reflections, we define  $P$  to be the parity operator such that at every reflection  $\phi'(x) = P\phi(x) = \phi(-x)$ , where  $\phi$  and  $\phi'$  are the light fields before and after the reflection respectively. This approach allows us to consider the scattering of incident light by a particle simply as operators acting on the input field. In our case it's not necessary to know the exact form of these operators, which makes it possible to consider particles of general size.

We assume that the incoming field amplitude distribution  $\phi_0$  is symmetric, i.e.  $P\phi_0 = \phi_0$ , and the field is p-polarized. Additionally, as mentioned before, the backscattered light from the particle is effectively canceled by the polarizer P, so we can ignore it completely in our analysis.

### 3.2 Beam propagation

After passing through the beamsplitter and propagating until the lens assembly as shown in figure 1, the clockwise and the counter-clockwise fields ( $\phi_{cw}$  and  $\phi_{ccw}$ ) take the form

$$\begin{aligned}\phi'_{cw} &= -r_p \exp(ikL_1)\phi_0 \\ \phi'_{ccw} &= t_p f_s \exp(ikL_2)\phi_0,\end{aligned}\tag{1}$$

where we used the symmetry of  $\phi_0$  and defined field transmission coefficients  $r_p = \sqrt{R_p}$  and  $t_p = \sqrt{T_p}$ . Here  $R_p$  and  $T_p$  are the intensity reflection and transmission coefficients of the beamsplitter for the p polarization and  $f_s = \sqrt{F_s}$  with  $F_s$  being the intensity transmission coefficient of the glass plate G.

After interacting with the particle, the light is scattered both forward and backward, given by the operators  $F[x_p]$  and  $B[x_p]$ , where  $x_p$  is a parameter that denotes the position of the particle along the  $x$  axis. These operators are defined so that after interacting with the particle, the fields become:

$$\begin{aligned}\phi''_{cw} &= F[x_p]\phi'_{cw} + B[-x_p]\phi'_{ccw} \\ \phi''_{ccw} &= F[-x_p]\phi'_{ccw} + B[x_p]\phi'_{cw}.\end{aligned}\quad (2)$$

A crucial detail is that the direction of  $\hat{\mathbf{x}}$  for the CW field is opposite to that of the CCW field, which is the reason for the different signs of  $x_p$ .

The CW and CCW beams are assumed to pass through  $m$  and  $n$  mirrors respectively after interacting with the particle. After the fields join again at the beamsplitter, the field in the dark port becomes

$$\begin{aligned}\phi_d &= \exp(ikL_2)P^{m+1}(f_p r_s F[x_p]\phi'_{cw} + f_s r_p B[-x_p]\phi'_{ccw}) + \\ &+ \exp(ikL_1)P^n(t_s F[-x_p]\phi'_{ccw} + t_p B[x_p]\phi'_{cw}),\end{aligned}\quad (3)$$

where the exponent  $(m+1)$  is due to the additional reflection from the beamsplitter.

The experiment is set up to ensure equal power in the CW and CCW fields in the trapping point, or equivalently,  $r_p = t_p f_s \equiv A$ . In addition, the backscattered light is filtered by the polarizer P. Then, equation (3) becomes

$$\phi_d = A \exp(ikL_2) \exp(ikL_1) (-r_s f_p P^{m+1} F[x_p] + t_s P^n F[-x_p]) \phi_0. \quad (4)$$

Since the beams are incident at nearly Brewster's angle onto the glass plate G,  $f_p \approx 1$ , so we will drop it in following equations.

We suppose that the relation  $PF[-x_p] = F[x_p]$  is satisfied, which is valid in particular when the particle is a homogeneous sphere and is trapped in the focal plane. Then, equation (4) can be simplified to be

$$\phi_d = A \exp(ik(L_1 + L_2)) ((t_s - r_s)F_s + ((-1)^m r_s - (-1)^n t_s)F_a) \phi_0, \quad (5)$$

where, without any loss of generality, we rewrote the operators in terms of their symmetric and antisymmetric parts:  $F[x_p] = F = F_a + F_s$  and  $B[x_p] = B = B_a + B_s$ . The subscripts indicate symmetry, i.e.  $PF_s = F_s$  and  $PF_a = -F_a$ .

From equation (5) it can be seen that in order to obtain constructive interference for the antisymmetric part of the forward scattered field, the total number of mirrors,  $(m+n)$ , must be odd, which is a general result for the forward scattered field.

In the particular case of a Rayleigh scatterer trapped at an antinode of the standing wave in the trapping plane, as studied by Taylor *et al.* [11], the forward scattering is the same as the backward scattering. Additionally the polarization is assumed to be the same through the setup, so we can write  $r_s = r_p$ ,  $t_s = t_p$ ,  $f_p = f_s = 1$ . When these hypotheses are applied to the equation (3), the resulting expression becomes

$$\phi_{d-ray} = -\exp(2ikL_1)((t^2 - r^2)F_s + (t+r)^2F_a)\phi_0, \quad (6)$$

which corresponds to the result of Taylor *et al.* [11], thus confirming our approach.

### 3.3 Signal enhancement

The signal-to-noise ratio is typically defined as the ratio between the variance of the signal and the variance of the noise:

$$SNR = \frac{\text{Var}(i_{signal})}{\text{Var}(i_{noise})}. \quad (7)$$

Following Taylor *et al.* [11], we notice that the laser powers typically used in optical trapping experiments exceed greatly the saturation threshold of commercial QPD detectors. For instance, we use the QP50-6 QPD by First Sensor which has a saturation threshold of approximately 1 mW. Therefore, the light field in the dark port has to be attenuated to reach an average power level just below the saturation threshold. Then, the comparison between Sagnac BFP and traditional BFP should be performed by assuming equal total incident power at the QPD.

Since the optical shot noise is a function of average light power incident on the detector and the average light power in our comparison is the same both for Sagnac and traditional BFP, we have

$$\begin{aligned} SNR_{sagnac} &= \frac{\text{Var}(i_{signal-sagnac})}{\text{Var}(i_{noise})}, \\ SNR_{bfp} &= \frac{\text{Var}(i_{signal-bfp})}{\text{Var}(i_{noise})}. \end{aligned} \quad (8)$$

Then, by using the definition of the signal-to-background ratio in terms of the averaged background

$$\text{Var}(i_{signal}) = (SBR \cdot \overline{i_{background}})^2, \quad (9)$$

we obtain

$$\frac{SNR_{sagnac}}{SNR_{bfp}} = \left( \frac{SBR_{sagnac}}{SBR_{bfp}} \right)^2. \quad (10)$$

Therefore, the measurements that we show in this work can be expressed equivalently as the signal-to-noise ratio (SNR) improvement or the signal-to-background ratio (SBR) improvement.

The signal amplitude and the background level is calculated by setting  $F_s \phi_0 = \phi_s$  and  $F_a \phi_0 = \phi_a$  and by assuming  $(m+n)$  to be odd. Then the equation 5 becomes

$$\phi_d(x) = A((t_s - r_s)\phi_s(x) + (t_s + r_s)\phi_a(x)) \quad (11)$$

up to a complex multiplier of unit modulus.

In order to calculate the signal-to-background ratio improvement, it is not necessary to integrate the intensity over  $x$ . Instead, we note the fact that the sum of intensities on a symmetrical pair of points  $\{-x, x\}$  is proportional to the total light power incident onto the QPD, and is given by

$$|\phi_d(x)|^2 + |\phi_d(-x)|^2 = 2((t_s - r_s)^2 |\phi_s|^2 + (t_s + r_s)^2 |\phi_a|^2) \approx 2(t_s - r_s)^2 |\phi_s|^2. \quad (12)$$

We used the experimentally valid hypothesis of sufficiently small oscillations of the particle, i.e.  $|\phi_a|^2 \ll |\phi_s|^2$ .

Analogously, the ‘‘X-signal’’ in the QPD detector is proportional to the difference of the intensities

$$|\phi_d(x)|^2 - |\phi_d(-x)|^2 = 4(T_s - R_s) \text{Re}(\phi_s \phi_a^*). \quad (13)$$

In our case of  $|\phi_a|^2 \ll |\phi_s|^2$  the signal-to-background (SBR) ratio becomes

$$k_{sbr-sagnac} \propto \frac{|\phi_d(x)|^2 - |\phi_d(-x)|^2}{|\phi_d(x)|^2 + |\phi_d(-x)|^2} = 2 \cdot \frac{t_s + r_s}{t_s - r_s} \cdot \frac{\text{Re}(\phi_s \phi_a^*)}{|\phi_s|^2}. \quad (14)$$

The degenerate case when  $t_s = t_p = 1$  and  $r_s = r_p = 0$  (i.e. no interferometer) corresponds to typical back-focal-plane interferometry. The signal-to-background ratio is then given by

$$k_{sbr-bfp} \propto \frac{|\phi_d(x)|^2 - |\phi_d(-x)|^2}{|\phi_d(x)|^2 + |\phi_d(-x)|^2} = 2 \cdot \frac{\text{Re}(\phi_s \phi_a^*)}{|\phi_s|^2}. \quad (15)$$

Therefore, the use of a Sagnac interferometer allows to improve the SBR over the typical back-focal-plane interferometry by a factor of

$$\frac{k_{sbr-sagnac}}{k_{sbr-bfp}} = \frac{t_s + r_s}{t_s - r_s}. \quad (16)$$

In our experimental case, expression (16) gives a maximum achievable SBR improvement factor of  $\approx 11.9$  given the transmission and reflection coefficients of the Thorlabs BSW26 beamsplitter ( $R_s \approx 56.47\%$ ,  $T_s = 40.68\%$ ).

## 4 Results and discussion

### 4.1 Particle generation and levitator-assisted trapping

The inkjet cartridge-based particle generation with evaporative diameter reduction proved to be reliable over several months of operation. Due to the abundance of nozzles (over 50) in the cartridge [9], problems with a non-working nozzle, e.g. due to clogging, were easily solved by using an alternative nozzle. By using a mixture of 5% glycerol in water, stable droplet generation of particles with a constant diameter of  $11 \pm 1 \mu\text{m}$  was achieved. Their sizes were measured by using diffraction patterns similar to the one shown in figure 5.

The levitation-assisted delivery greatly simplified the trapping of droplets into the horizontal counter-propagating optical tweezers. The illumination of the whole stream of falling droplets, as in figure 3, provided us with a visual feedback on the cartridge’s orientation during fine adjustments. Normally, 30-50 droplets had to be generated to finely adjust the cartridge orientation in order to compensate for mechanical drifts. After this adjustment all the subsequent droplets descended into the levitator trap where they were trapped. By eliminating the remaining long-term mechanical drifts, it should be possible to achieve automatic “trap on demand” operation with single droplets.

### 4.2 Position measurement and improvement of signal-to-background ratio

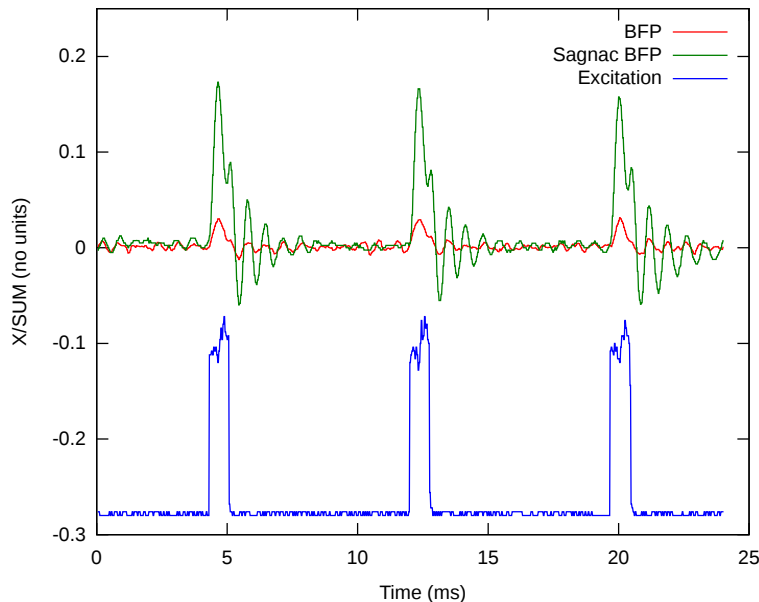


Figure 6: Comparison between the normalized position signals obtained with the traditional BFP interferometry (red) and Sagnac-enhanced BFP interferometry (green). The side-pressure laser power (blue, arbitrary units) is driven by a 10% duty cycle, 130 Hz TTL wave.

The signal that we obtained was normalized to be consistent with equation (14), i.e is the ratio of the signals obtained from the QPD detector

$$x_{norm} = \frac{X}{SUM}, \quad (17)$$

where  $X$  is the difference of power between the left and right halves of the QPD detector and  $SUM$  is the total power arriving at the detector. The data expressed in this way is effectively the signal divided by the background and thus, can be used directly to compare the typical BFP measurements to the Sagnac-enhanced BFP measurements.

Figure 6 shows typical curves of the normalized position signals, as specified by the equation (17). The side pressure laser is applied with a frequency of 130 Hz and duty cycle of 10%. The red curve in the figure displays the measured normalized position using the BFP interferometry whereas the green curve displays the same quantity using Sagnac-enhanced BFP interferometry.

The particle position signal shows a typical response of an underdamped harmonic oscillator to a periodic rectangular-wave external force (blue curve in figure 6). This is expected as the damping ratio is much less than one for a 10-micrometer particle in air trapped in optical tweezers with a total laser power of 1W. The small structure during the laser-on period, shown as two small bumps in the power signal (blue) is due to mode-jumping in the side-pressure laser during the modulation. These power fluctuations give rise to similar bumps in the particle position (green and red).

Signals obtained by the Sagnac-enhanced BFP and typical BFP are multiples of one another, as shown in 3.3, and it is enough to simply consider the ratio between the two signals to calculate the SBR improvement. An enhancement of  $5.6 \pm 0.1$  was obtained when comparing the Sagnac-enhanced back focal plane interferometry with the typical back focal plane interferometry. The theoretical limit for the improvement, as calculated in section 3.3, is approximately 11.9. In practice, this value will be reduced due to the non-idealities of the setup, such as the sub-optimal performance of our aspherical lenses at a wavelength of 532 nm and the imperfect mode matching in the interferometer. Compared to typical back focal plane interferometry, the signal-to-shot-noise improvement corresponding to our measurements is more than 30-fold according to equation (10).

## 5 Conclusion

We have extended the theory by Taylor *et al.* [11] to a case of arbitrarily-sized spherical particles trapped in orthogonally-polarized counter-propagating optical tweezers. We experimentally demonstrated a significant improvement in the signal-to-background ratio for position detection of 11  $\mu\text{m}$ -sized particles by embedding counterpropagating optical tweezers into a Sagnac interferometer. The results are consistent with the theoretical prediction, thus validating our approach. The obtained data indicates an increase of signal-to-shot-noise ratio of more than 30 times compared to typical back focal plane interferometry.

We have constructed a system based on a low-cost commercial inkjet cartridge [9] and an optical levitator [3] that could efficiently generate, trap and guide into the optical tweezers single glycerol droplets in air, while having precise evaporation-based control over the droplet size. By eliminating the remaining long-term mechanical drifts in this system, it should be possible to achieve automatic “trap on demand” operation with single droplets.

We hope that our results will be useful for experiments requiring an improved resolution in the BFP interferometry position detection for spherical particles in the Mie and geometrical optics regimes, such as the counterpropagating setup for center-of-mass motion cooling of 3  $\mu\text{m}$  particles in Ref. [6].

## 6 Acknowledgments

We thank José Luis Meza for his invaluable assistance during the development of the project in the Faculty of Sciences, UNAM. This work was supported by the Carl Trygger foundation for Scientific Research,

the Linnaeus-Palme International Exchange Program and by the grant "Bottlenecks for particle growth in turbulent aerosols" from the Knut and Alice Wallenberg Foundation, Dnr. KAW 2014.0048.

## References

- [1] A. Ashkin and J. M. Dziedzic. Optical levitation by radiation pressure. *Applied Physics Letters*, 19(8):283–285, 1971.
- [2] A. Ashkin, J. M. Dziedzic, J. E. Bjorkholm, and Steven Chu. Observation of a single-beam gradient force optical trap for dielectric particles. *Opt. Lett.*, 11(5):288–290, May 1986.
- [3] Robert C. Gauthier and Athanasios Frangioudakis. Optical levitation particle delivery system for a dual beam fiber optic trap. *Appl. Opt.*, 39(1):26–33, Jan 2000.
- [4] Frederick Gittes and Christoph F. Schmidt. Interference model for back-focal-plane displacement detection in optical tweezers. *Opt. Lett.*, 23(1):7–9, Jan 1998.
- [5] Günter Georg Hoffmann, Emil Lentz, and Bernhard Schrader. Simple device for the generation and optical levitation of single aerosol particles. *Review of Scientific Instruments*, 64(3):823–824, 1993.
- [6] Tongcang Li, Simon Kheifets, and Mark G. Raizen. Millikelvin cooling of an optically trapped microsphere in vacuum. *Nature Phys.*, 7:527–530, 2011.
- [7] M. Nazarathy and J. Shamir. Fourier optics described by operator algebra. *J. Opt. Soc. Am.*, 70(2):150–159, Feb 1980.
- [8] M. Ribezzi-Crivellari, J. M. Huguet, and F. Ritort. Counter-propagating dual-trap optical tweezers based on linear momentum conservation. *Review of Scientific Instruments*, 84(4):–, 2013.
- [9] Aleksandr V Sergeev and Raymond A Shaw. An inexpensive uniform-size aerosol generator. *Measurement Science and Technology*, 17(10):N41, 2006.
- [10] Karel Svoboda, Christoph F. Schmidt, Bruce J. Schnapp, and Steven M. Block. Direct observation of kinesin stepping by optical trapping interferometry. *Nature*, 365(6448):721–727, October 1993.
- [11] M A Taylor, J Knittel, M T L Hsu, H-A Bachor, and W P Bowen. Sagnac interferometer-enhanced particle tracking in optical tweezers. *Journal of Optics*, 13(4):044014, 2011.